

ARTICLE

Received 22 Jul 2016 | Accepted 25 Dec 2016 | Published 16 Feb 2017

DOI: 10.1038/ncomms14408

OPEN

# Zero-gap semiconductor to excitonic insulator transition in $\text{Ta}_2\text{NiSe}_5$

Y.F. Lu<sup>1</sup>, H. Kono<sup>1</sup>, T.I. Larkin<sup>2</sup>, A.W. Rost<sup>2,3</sup>, T. Takayama<sup>2</sup>, A.V. Boris<sup>2</sup>, B. Keimer<sup>2</sup> & H. Takagi<sup>1,2,3</sup>

The excitonic insulator is a long conjectured correlated electron phase of narrow-gap semiconductors and semimetals, driven by weakly screened electron-hole interactions. Having been proposed more than 50 years ago, conclusive experimental evidence for its existence remains elusive.  $\text{Ta}_2\text{NiSe}_5$  is a narrow-gap semiconductor with a small one-electron bandgap  $E_G$  of  $<50$  meV. Below  $T_C = 326$  K, a putative excitonic insulator is stabilized. Here we report an optical excitation gap  $E_{\text{op}} \sim 0.16$  eV below  $T_C$  comparable to the estimated exciton binding energy  $E_B$ . Specific heat measurements show the entropy associated with the transition being consistent with a primarily electronic origin. To further explore this physics, we map the  $T_C$ - $E_G$  phase diagram tuning  $E_G$  via chemical and physical pressure. The dome-like behaviour around  $E_G \sim 0$  combined with our transport, thermodynamic and optical results are fully consistent with an excitonic insulator phase in  $\text{Ta}_2\text{NiSe}_5$ .

<sup>1</sup>Department of Physics, University of Tokyo, Bunkyo-ku, Tokyo 113-0033, Japan. <sup>2</sup>Max Planck Institute for Solid State Research, Heisenbergstrasse 1, 70569 Stuttgart, Germany. <sup>3</sup>Institute for Functional Matter and Quantum Technologies, University of Stuttgart, Pfaffenwaldring 57, 70550 Stuttgart, Germany. Correspondence and requests for materials should be addressed to A.W.R. (email: andreas.rost@fmq.uni-stuttgart.de) or to H.T. (email: h.takagi@fkf.mpg.de).

Formation of exotic electronic phases driven by electron correlations is among the most intriguing phenomena in condensed matter physics. One such many-body ground state is the excitonic insulator being stabilized in materials where the conduction and valence band are either separated by a small energy gap (semiconductors) or are overlapping in energy by a small amount (semimetals). In narrow-gap semiconductors and semimetals, the Coulomb interaction between electrons and holes may lead to a spontaneous formation of electron–hole pairs, namely, excitons<sup>1–4</sup>. These charge neutral pairs can in analogy to superconductivity give rise to an unconventional insulating ground state—the excitonic insulator—which is characterized by a many-body gap  $2\Delta_E$  opening in the single particle excitation spectrum (Fig. 1a).  $2\Delta_E$  mirrors the exciton binding energy  $E_B$ .

The excitonic state is thermodynamically most stable for a zero-gap semiconductor  $E_G = 0$ . Reducing  $E_G$  to a negative value (the semimetallic region) increases the electron/hole density in the one-electron band structure due to band overlap. The increased carrier density screens the effective Coulomb interaction between electrons and holes, and consequently suppresses the stability of excitonic pairs and therefore  $T_C$ . This is in strong contrast to a simple hybridization gap, which also exists for a large band overlap. For positive  $E_G$  (the semiconducting phase), the spontaneous formation of excitons is suppressed with increasing  $E_G$  and the excitonic phase becomes unstable against the semiconducting ground state for  $E_G \sim E_B$  (refs 2,4). In the semimetallic negative  $E_G$  region where interactions are well screened and weak, the transition may be described by BCS mean-field theory due to the analogy with superconductivity<sup>2,4–6</sup>. On going to the positive  $E_G$  region, one crosses over to a BEC-like limit as a consequence of strong coupling. This BCS–BEC

crossover might be reflected in  $2\Delta_E/k_B T_C$  being strongly enhanced over the BCS weak coupling value. In Fig. 1a, we schematically show the generally predicted phase diagram with its characteristic dependence of the excitonic transition temperature  $T_C$  on the one electron bandgap  $E_G$  (refs 2,4).

Candidate materials previously discussed include  $\text{TmSe}_{0.45}\text{Te}_{0.55}$  (refs 7–9) and  $1T\text{-TiSe}_2$  (refs 10,11). In both cases, transitions to possible excitonic insulator phases were observed. These transitions are however accompanied by strong finite  $\mathbf{q}$  lattice distortions as expected in the excitonic scenario for such indirect-gap semiconductors. Analysis of the entropy changes involved based on specific heat showed that the transitions in these materials are driven not only by the small number of electrons and holes but are strongly influenced by lattice and spin degrees of freedom<sup>12,13</sup>. This is in contrast to the excitonic insulator limit, where lattice deformations play a secondary role<sup>1–6,14</sup>. Alternative scenarios such as a charge density wave or a band Jahn–Teller effect, which were put forward especially for  $1T\text{-TiSe}_2$  (refs 15,16), can therefore not be excluded to describe the relevant physics of these materials, leaving room for question on the existence of a canonical excitonic insulator phase.

$\text{Ta}_2\text{NiSe}_5$ , first reported by Sunshine *et al.*<sup>17</sup> and Di Salvo *et al.*<sup>18</sup>, is a layered compound stacked by van der Waals interactions and crystallizing in an orthorhombic  $Cmcm$  structure above  $T_C$ , as illustrated in Fig. 1b,c (ref. 18). Each layer is composed of parallel chains of edge-shared  $\text{TaSe}_6$  octahedra and corner-shared  $\text{NiSe}_4$  tetrahedra, running along the crystallographic  $a$  axis.

Band structure calculations in the orthorhombic high-temperature phase of  $\text{Ta}_2\text{NiSe}_5$  show that the conduction band

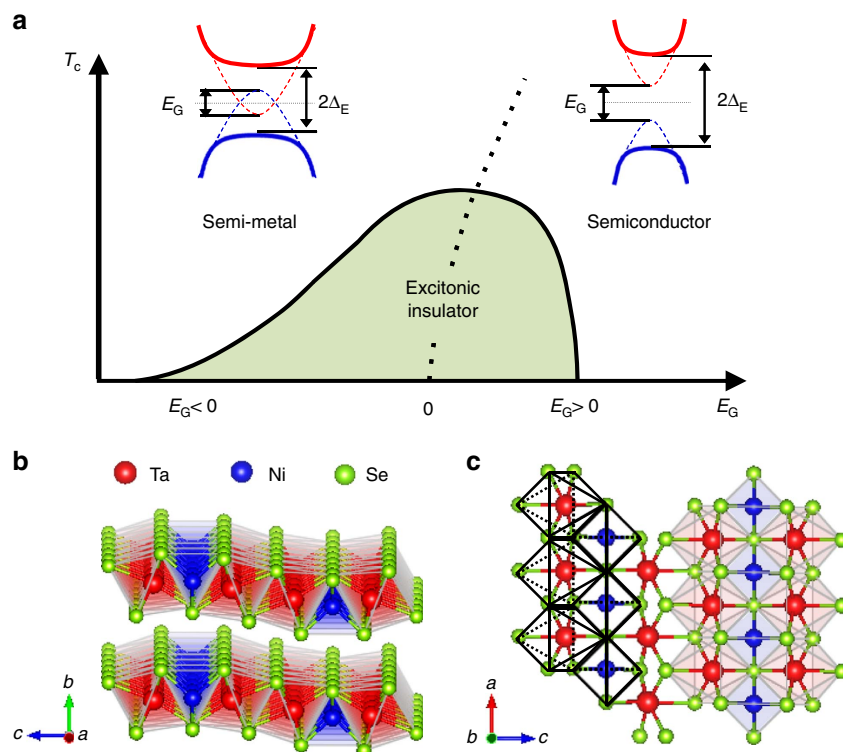


**Figure 1 | Excitonic insulator and  $\text{Ta}_2\text{NiSe}_5$  structure.** (a) Schematic phase diagram of excitonic gap formation as a function of  $E_G$ . The dotted line indicates the crossover from semimetallic to semiconducting behaviour. The insets show the relation between  $E_G$  and  $\Delta_E$  for the metallic and insulating limits.  $E_G$  is the one-electron bandgap between conduction (red) and valence band (blue). The Coulomb interaction between electron- and hole-like excitations can lead to electron–hole pairing (exciton formation) and the opening of a new many-body excitation gap  $\Delta_E$  in the excitonic insulator phase. (b) The orthorhombic phase of  $\text{Ta}_2\text{NiSe}_5$  shown in two orientations emphasizing the layered nature in the  $a$ – $c$  plane, and (c) the  $\text{TaSe}_6$  and  $\text{NiSe}_4$  chains along the  $a$  direction (right).

minimum and the valence band maximum are almost degenerate at the  $\Gamma$  point<sup>14,19</sup> implying a very small direct gap  $E_G$ . The valence band is composed of Ni 3d orbitals with a Se 4p admixture while Ta 5d orbitals dominate the conduction bands. Note that the valence and the conduction bands in the orthorhombic phase belong to different irreducible representations of the crystal structure<sup>14,19</sup>. The formation of a single particle hybridization gap is therefore forbidden by crystal symmetry.

The small direct gap semiconductor realised in Ta<sub>2</sub>NiSe<sub>5</sub> above  $T_C$  is an ideal situation for the formation of an excitonic insulator phase. A semiconductor-to-insulator transition is indeed observed at  $T_C \approx 326$  K (ref. 18). This is accompanied by a very weak  $\mathbf{q}=0$  structural phase transition to monoclinic  $C2/c$  with the unit cell size remaining the same across the transition and whose small magnitude cannot account for the observed electronic changes<sup>14</sup>. This excludes a lattice distortion-mediated charge density wave mechanism driving the phase formation, as discussed in the case of Mo bronze<sup>20</sup>, suggesting it to be electronic in origin<sup>14</sup>. Recent X-ray photoemission spectroscopy (XPS) and angle-resolved photoemission spectroscopy (ARPES) measurements revealed a flattening of the valence band below  $T_C$ , which was interpreted as the formation of an additional gap<sup>21</sup>. Based on these observations, the low-temperature phase was proposed to be an excitonic insulator. Ta<sub>2</sub>NiSe<sub>5</sub> is distinct from other excitonic insulator candidates. First, due to the direct gap, the excitonic states do not require a finite  $\mathbf{q}$  super-lattice modulation and can be accessed easily by optical spectroscopy. Second, electrons in Ta chains and holes in Ni chains are spatially separated in real space, which could stabilize the excitonic pair and hence the excitonic insulator.

Recognizing its uniqueness as a candidate excitonic insulator, electric transport, optical and specific heat measurements as well as physical and chemical pressure experiments were conducted on Ta<sub>2</sub>NiSe<sub>5</sub> single crystals to test the validity of the excitonic insulator scenario. We will demonstrate that Ta<sub>2</sub>NiSe<sub>5</sub> is a nearly zero-gap semiconductor at high temperatures with an optical gap  $E_{op} \sim 0.16$  eV, comparable to the expected excitonic binding energy  $E_B$ , developing below  $T_C = 326$  K. The majority of entropy change at the transition appears to originate from thermally excited electrons and holes consistent with the thermodynamics of phase formation to be dominated by electronic degrees of freedom. The physical and chemical pressure experiments indicate the suppression of  $T_C$  both by moving towards negative (semimetal) and positive (semiconductor) bandgap  $E_G$  resulting in a dome-shaped  $T_C$  versus  $E_G$  curve around  $E_G = 0$ . All these results are consistent with those expected for a canonical excitonic insulator.

## Results

**Zero-gap semimetal-to-semiconductor transition.** The transition in Ta<sub>2</sub>NiSe<sub>5</sub> crystals is most readily seen in transport as shown in Fig. 2a. Here we present the resistivity  $\rho_a$  parallel to the Ta and Ni chains ( $I \parallel a$  axis) as a function of temperature. A weak but well-defined kink is observed at  $T_C = 326$  K. This agrees well with previous reports<sup>18</sup>. At high temperatures, the resistivity is essentially temperature independent over a wide range from 400 to 550 K. This means the transport gap is at most of the order of  $\sim 0.05$  eV, suggestive of an almost zero energy gap above  $T_C$ . Right below  $T_C$ , the resistivity increases rapidly, suggesting the opening of an additional gap. It is instructive for an excitonic insulator transition to present the data in form of an activation energy plot showing  $E_p = -k_B T^2 (\partial \ln \rho / \partial T)$  as a function of temperature (Fig. 2b; Supplementary Fig. 1).  $E_p$  reflects an activation energy  $E_A$  if the temperature dependence at a given temperature is approximated by a thermally activated behaviour

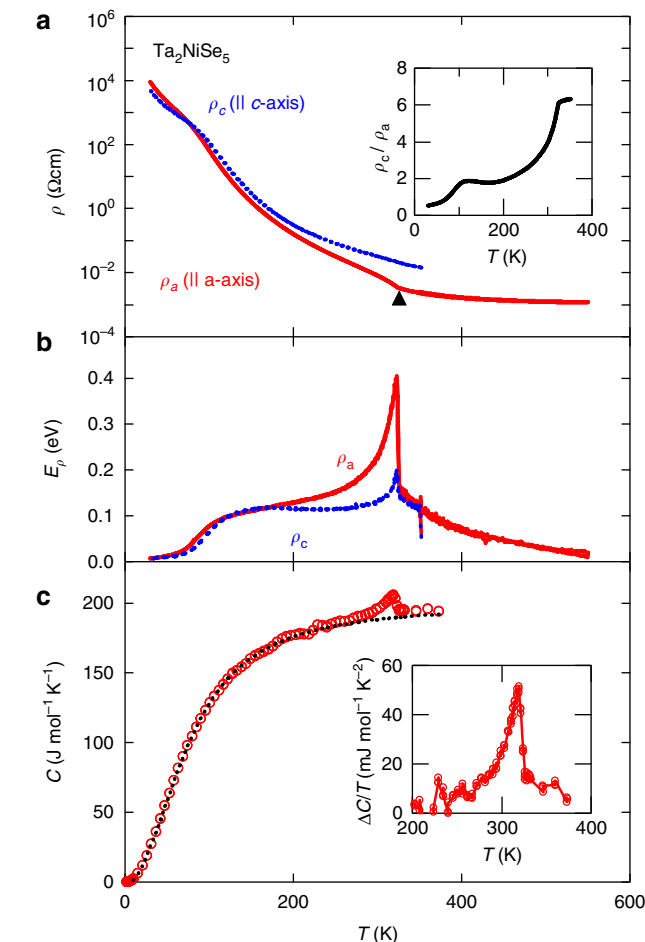


**Figure 2 | Ta<sub>2</sub>NiSe<sub>5</sub> transport and specific heat.** (a) Temperature dependence of the in-plane resistivity of Ta<sub>2</sub>NiSe<sub>5</sub> single crystal  $\rho_a$  (red) along the  $a$  axis parallel to the Ta and Ni chains, and  $\rho_c$  (blue) along the  $c$  axis perpendicular to the chains. An anomaly is observed at  $T_C = 326$  K (emphasized by black triangle). The inset shows the temperature dependence of the resistivity ratio,  $\rho_c/\rho_a$  as an indicator of the in-plane anisotropy. (b) The temperature dependence of the activation energy  $E_p$  of the resistivity data in **a** given by  $E_p = -k_B T^2 (\partial \ln \rho / \partial T)$ . (c) Temperature dependence of heat capacity  $C$  of a Ta<sub>2</sub>NiSe<sub>5</sub> single crystal. An anomaly in  $C$  at  $T_C$  is clearly visible. The phonon contribution (black dashed line) is roughly estimated from a Debye fit to the low-temperature data below  $T_C$ . The inset shows the excess specific heat  $\Delta C/T$  around  $T_C$  obtained from the raw heat capacity by subtracting the lattice contribution.

$\rho = \rho_0 \exp(-E_A/k_B T)$  and therefore mirrors the energy scale of thermal excitation of charge carriers.  $E_p$  shows a clear jump at  $T_C$  consistent with theoretical calculations<sup>4,22</sup>, predicting a step-like increase of  $E_p$  at  $T_C$ .  $E_p$  below the jump is 0.1–0.2 eV, which suggests a gap of the order of a few tenths of an eV opening below  $T_C$ . At lower temperature below 100 K, we observe a suppressed activation energy  $E_p$ . In this temperature regime, the conduction due to impurity states, with much lower energy scale of charge excitations, very likely dominates the temperature dependence.

The resistivity perpendicular to the layer is orders of magnitude higher than the in-plane resistivity and we were not able to obtain a reliable estimate of the out-of-plane resistivity. Reflecting the presence of quasi-one-dimensional Ta and Ni chains, a moderate in-plane anisotropy is observed. As shown in Fig. 2a, above  $T_C$ , the resistivity perpendicular to the chains ( $I \parallel c$  axis),  $\rho_c$ , is larger than  $\rho_a$  along the chains by a factor of 6, indicating weak but appreciable electronic quasi-one-

dimensionality. Below  $T_C$ , this quasi-one-dimensionality in transport appears to be washed out, suggesting that the excitonic gap formation makes charge transport isotropic. This isotropy might be related to the flattening of the one-dimensional

dispersion. We note that such temperature dependence in the  $\rho_c/\rho_a$  plot is absent in the family compound  $Ta_2NiS_5$ , which does not show any signature of an excitonic-like transition (Supplementary Fig. 2).

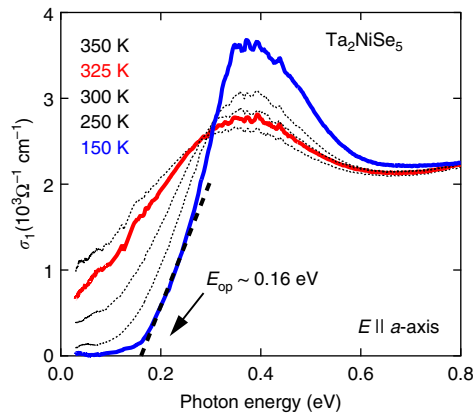


**Figure 3 | Optical conductivity.** Optical conductivity spectra of  $Ta_2NiSe_5$  single crystal at various temperatures, showing the opening of a charge excitation gap associated with the transition at  $T_C = 326$  K. The gap of  $E_{op} \approx 0.16$  eV is estimated from the usual extrapolation of the linear regime of conductivity (black dashed line). The electric polarization was parallel to the  $a$  axis.

**Gap formation below  $T_C$ .** An additional many-body excitation gap  $2\Delta_E$  should open at  $T_C$  due to the excitonic transition. While ARPES<sup>21</sup> measurements are consistent with such a gap opening, a complete picture of the gap formation has not been unveiled yet due to the limitation of the measurement to occupied states below the Fermi level and the restricted temperatures at which the experiments were carried out. The formation of an excitation gap at  $T_C$  is much more clearly evidenced by the optical conductivity spectrum with photon polarization along the chain direction  $a$  shown in Fig. 3. At high temperatures above  $T_C$ , a broad continuum is observed with a hump-like structure around 0.3–0.4 eV, which is consistent with  $Ta_2NiSe_5$  being an almost zero-gap semiconductor. On cooling below  $T_C$ , the spectral weight is transferred from below an isosbestic point of  $E^* \sim 0.3$  eV to higher energies with a full gap of  $E_{op} \sim 0.16$  eV forming. At 150 K, a gap structure with an absorption peak at 0.4 eV is well established. The opening of a gap is further demonstrated by the temperature evolution of the conductivity at an energy well below the gap which we show in the Supplementary Fig. 3. According to the previous ARPES study, the band maximum relative to the Fermi energy—the effective valence band gap—was estimated to

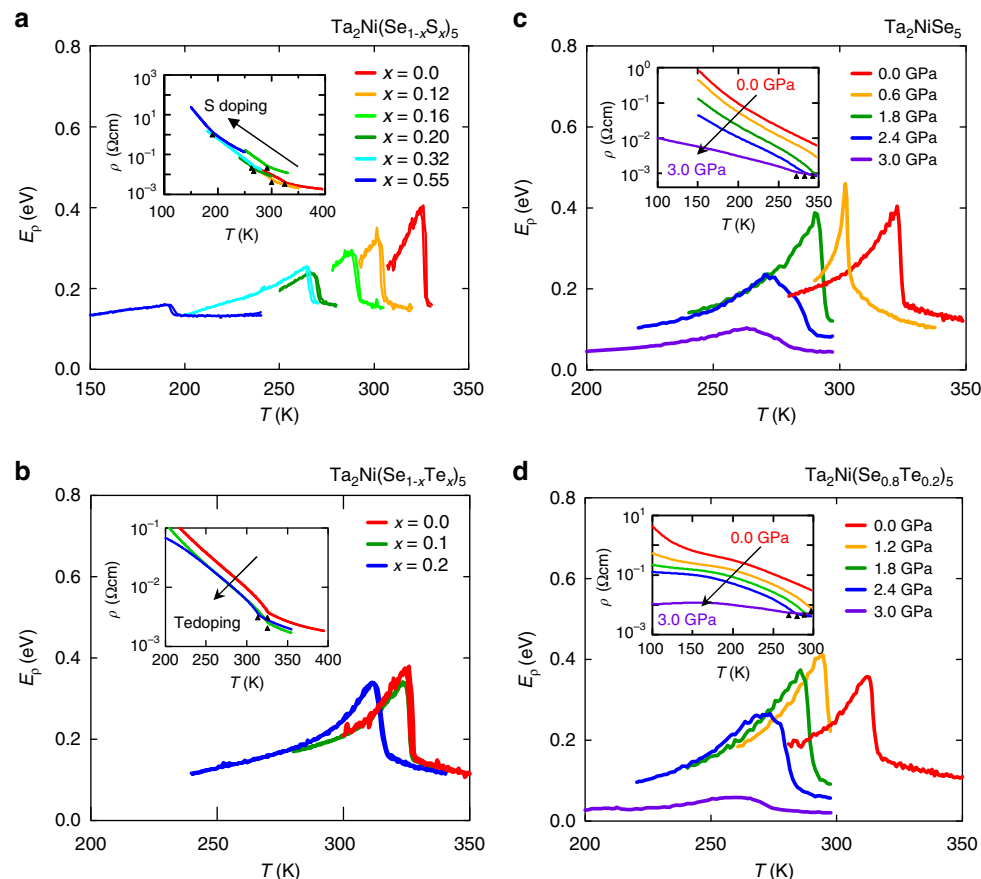


**Figure 4 | Chemical and physical pressure.** (a) The activation energy plot  $E_p = -k_B T^2 (\partial \ln \rho / \partial T)$  for  $Ta_2Ni(Se_{1-x}S_x)_5$  that clearly shows the systematic shift of  $T_C$  with S doping. The inset shows resistivity curves ( $I \parallel a$  axis) as a function of temperature. Triangles mark the transition temperatures for each sample. Variations in absolute values are due to uncertainties in, for example, exact sample dimensions. In (b), we show the equivalent data for the  $Ta_2Ni(Se_{1-x}Te_x)_5$  series. (c) The activation energy plot as a function of temperature for a single high-pressure experiment showing both the systematic reduction of  $E_p$  with pressure as well as the suppression of  $T_C$ . Additional data from a high-temperature run are also included. The inset shows the equivalent resistivity data with emphasis of  $T_C$  by triangles. (d) Equivalent data to (c) for  $Ta_2Ni(Se_{0.8}Te_{0.2})_5$ .



be 0.17 eV, which is roughly consistent with the characteristic energy for spectral weight transfer (isosbetic point)  $E^* \sim 0.3$  eV and the optical gap  $E_{op} \sim 0.16$  eV in the optical conductivity.

**Thermodynamic signature of phase transition.** A clear anomaly in the specific heat  $C(T)$  can be identified at  $T_C$  (Fig. 2c), with the shape being reminiscent of a BCS-type superconducting transition. This constitutes thermodynamic evidence for the opening of a gap in the electronic excitation spectrum at this transition. The entropy associated with the transition is roughly  $\Delta S \sim 0.3 \text{ J mol}^{-1} \text{ K}^{-1}$ . The density of states  $D$  at the quasi-one-dimensional band edge is of the order of 1 state per eV per unit formula<sup>14</sup>, yielding a rough estimate of density of electrons and holes at  $T_C = 326 \text{ K}$  of  $D \times k_B T_C \sim 0.03$  per unit formula in the zero-gap case. This is not inconsistent with the Hall coefficient  $+R_H \sim 10^{-2} \text{ cm}^3 \text{ C}^{-1}$  (hole like) measured at  $T_C$  (Supplementary Fig. 4), neglecting the ambiguity arising from the coexistence of electrons and holes. The quenched entropy of  $3k_B$  for 0.03 carriers corresponds to an entropy change  $\Delta S \sim 0.03 \times 3R = 0.7 \text{ J mol}^{-1} \text{ K}^{-1}$ , agreeing with the experimental value within a factor of 2. This rough estimate implies that the majority of entropy change associated with the transition and therefore the thermodynamically relevant degrees of freedom originate from the electronic entropy indicating an electronically driven phase transition.

**Phase diagram as a function of energy gap.** The isoivalent substitution of Se with Te and S was conducted to control the bandgap  $E_G$ .  $\text{Ta}_2\text{NiS}_5$  has compared with the isostructural  $\text{Ta}_2\text{NiSe}_5$  a larger transport activation energy of  $E_p \sim 0.2$  eV in resistivity (inset, Fig. 5), indicative of the presence of a much larger bandgap  $E_G$  than in  $\text{Ta}_2\text{NiSe}_5$ . As discussed, band calculations indicate that the valence band of  $\text{Ta}_2\text{NiSe}_5$  is composed of Ni  $3d$  and Se  $4p$  orbitals<sup>14</sup>. With increased S-substitution, the hybridization between Ni  $3d$  and Se  $4p$  (S  $3p$ ) orbitals are weakened. This lowers the energy of the states at the top of the valence band while the conduction band is less affected, resulting in an overall enhancement of the bandgap  $E_G$  compared to  $\text{Ta}_2\text{NiSe}_5$ . Changes in the Ta-chalcogen hybridization further enhance the band gap with increasing S-substitution but are predominantly affecting the energetically higher lying Ta- $d$  bands above 1 eV (ref. 23). Tellurium doping, on the other hand, pushes the system in the opposite direction, likely bringing the nearly zero gap of  $\text{Ta}_2\text{NiSe}_5$  to a negative region. Single crystals of the isoivalent series  $\text{Ta}_2\text{Ni}(\text{Se}_{1-x}\text{S}_x)_5$  and  $\text{Ta}_2\text{Ni}(\text{Se}_{1-x}\text{Te}_x)_5$  were grown. Te doping was limited up to  $x = 0.2$  due to the solubility limit likely due to the much larger ionic radius of Te.

We show the activation energy plot of resistivity for  $\text{Ta}_2\text{Ni}(\text{Se}_{1-x}\text{S}_x)_5$  and  $\text{Ta}_2\text{Ni}(\text{Se}_{1-x}\text{Te}_x)_5$  in Fig. 4a,b, respectively. It is clear that both by increasing and by decreasing the band gap  $T_C$  is suppressed, meaning  $T_C$  is peaked for  $\text{Ta}_2\text{NiSe}_5$  with a nearly zero bandgap. The inset of Fig. 5 shows the evolution of the activation energy  $E_{550\text{K}}$  for  $\text{Ta}_2\text{Ni}(\text{Se}_{1-x}\text{S}_x)_5$  estimated from high-temperature data in the temperature range of 500–550 K well above  $T_C$  (Supplementary Fig. 1), which should be closely related to the bandgap  $E_G$ . It is monotonically increasing and can be described by a linear correlation to leading order as shown, implying the continuous and almost linear increase of the bandgap  $E_G$  upon S-substitution. As  $E_{550\text{K}}$  is systematically enhanced with increasing S-substitution,  $T_C$  is suppressed to lower temperatures and eventually, for  $x > 0.55$ , no phase transition was observed in the temperature dependent resistivity down to 2 K. For  $\text{Ta}_2\text{Ni}(\text{Se}_{1-x}\text{Te}_x)_5$ , the decrease of resistivity at 350 K by  $\sim 70\%$  for  $x = 0.1$  and 0.2, respectively, indicates the continuous suppression of the energy gap (Fig. 4b). Although the

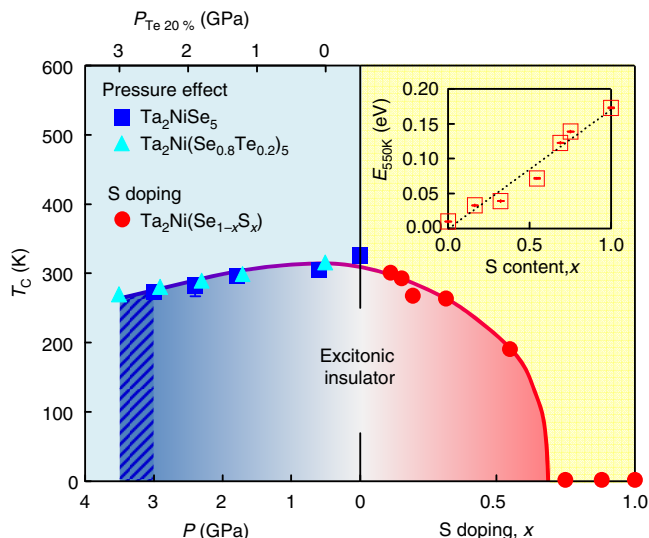


**Figure 5 | Phase diagram.** Phase diagram of the excitonic insulator phase in  $\text{Ta}_2\text{NiSe}_5$  given by the transition temperature  $T_C$  as a function of S doping (right) and pressure and Te doping (left), corresponding to the semiconducting and the semimetallic regions in the predicted phase diagram respectively. The pressure effect on  $\text{Ta}_2\text{Ni}(\text{Se}_{0.8}\text{Te}_{0.2})_5$  is also shown in the left region with an offset of chemical pressure of 0.5 GPa (see text). The shaded area in the left region indicates the region for phase separation behaviour at high pressures (see text), likely originating from a first-order transition. The inset shows the S doping  $x$  dependence of the transport activation energy of resistivity at high temperatures (500–550 K),  $E_{550\text{K}}$ .  $E_{550\text{K}}$  gives a measure of the one electron gap  $E_G$  and indicates that  $E_G$  increases monotonically as a function of  $x$  from almost zero for  $x = 0$  to at least a few tenths of an eV for  $x = 1.0$ . The universal substitution level  $x$  and pressure  $P$  may therefore be mapped onto the single band gap  $E_G$  in the high-temperature phase.

range of substitution is limited, the plot of  $E_p$  indicates a small but well resolved decrease of  $T_C$ .

To confirm the suppression of  $T_C$  by decreasing  $E_G$  towards the negative side, namely by Te-substitution, physical pressure was applied to  $\text{Ta}_2\text{NiSe}_5$ . As can be seen from the activation energy plot in Fig. 4c, a clear decrease of  $T_C$  is observed with increasing pressure. At 2.5 GPa,  $T_C$  is decreased from 326 to 280 K, corresponding to a  $T_C$  suppression rate of  $\sim 20 \text{ K GPa}^{-1}$ , which can be reasonably ascribed to the decrease of the energy gap in the negative gap region. With 20% of Te-substitution,  $T_C$  is reduced by 10 K, which is equivalent to 0.5 GPa of pressure. We performed the same pressure experiment also on 20% substituted  $\text{Ta}_2\text{Ni}(\text{Se}_{0.8}\text{Te}_{0.2})_5$  and observed again the suppression of  $T_C$  with a rate of  $\sim 20 \text{ K per GPa}$  (Fig. 4d). Therefore, once we offset an effective chemical pressure equivalent to 0.5 GPa, the two  $T_C(P)$  curves for pure and 20% Te substitute crystals fall onto a universal curve, strongly suggesting that the phase transition is controlled by a single parameter  $E_G$ . In the pressure range above 2.4 GPa, we observe that upon increasing pressure further the transition temperature does not shift significantly, while the magnitude of the anomaly is substantially suppressed (Fig. 4c,d) and conductivity in the low-temperature limit is significantly enhanced, suggestive of a first-order phase transition and the resultant phase coexistence. A recent pressure study up to 10 GPa on  $\text{Ta}_2\text{NiSe}_5$  indeed indicates that there is a first-order structural phase transition at  $P_C \sim 2.5$  GPa, and the system becomes metallic above  $P_C$ <sup>24</sup>. A reduction of resistivity under pressure is also measured for  $\text{Ta}_2\text{NiS}_5$  but no phase transition was observed up to 3 GPa.

The control of  $T_C$  by changing  $E_G$  via chemical substitution and physical pressure effects can be summarized in the phase diagram shown in Fig. 5, where the pressure is a measure of decreasing  $E_G$  on the negative  $E_G$  side and the S-substitution is the measure of increasing  $E_G$  on the positive side. Te-substitution was converted to equivalent pressure on the pressure axis. We clearly see the expected dome-shaped dependence of  $T_C$  around  $E_G \sim 0$  ( $\text{Ta}_2\text{NiSe}_5$ ).

## Discussion

The high-temperature phase of  $\text{Ta}_2\text{NiSe}_5$  appears to be very close to a zero-gap semiconductor making it an ideal candidate system for the stabilization of an excitonic insulator phase. Our optical data indeed show that below the phase transition temperature of  $T_C = 326$  K, a gap  $E_{\text{op}} \sim 0.16$  eV develops in the excitation spectrum consistent with the enhanced activation energy observed in our transport data. Significant spectral weight shifts occur from below the isosbestic point of  $\sim 0.3$  eV to higher energy scales of up to  $\sim 0.6$  eV. These energy scales should reflect the characteristic energy scales of the excitonic insulator and in particular experimentally constrains the scale of the exciton binding energy  $E_B$  to be of the order of a few tenths of an eV. Expressed in terms of an effective temperature (0.1 eV corresponding to  $\approx 1,000$  K)  $E_B$  is significantly larger than the experimental transition temperature to the excitonic insulator phase at 326 K, enabling the formation of this phase in  $\text{Ta}_2\text{NiSe}_5$ .

The exciton binding energy  $E_B$  of the order of a few tenths of an eV is orders of magnitude larger as compared with those of conventional three-dimensional semiconductors. However, we argue that the unusual properties of  $\text{Ta}_2\text{NiSe}_5$  explain at least in part the enhanced  $E_B$ . The excitonic binding energies can be captured by  $E_B = -13.6 \text{ eV} \mu / m_0 \epsilon^2$ . In this Rydberg formula,  $\mu$  is a material specific effective mass and  $\epsilon$  an effective permittivity<sup>25</sup>. First of all the  $d$ -band character of conduction (Ta  $5d$ ) and valence bands (Ni  $3d$ ) result in an effective reduced mass  $\mu$  of the order of  $m_0$  as can be determined from ARPES data<sup>21</sup> and band structure calculations<sup>14</sup>. This reduced mass is up to two orders of magnitude larger than in conventional direct gap semiconductors<sup>26</sup>. Furthermore the effective low dimensionality of the band structure and resulting physical properties are known to generally lead to a strong increase of the exciton binding energy<sup>26</sup>. Taken together, these effects can be expected to lead to a large enhancement of the exciton binding energy to a value consistent with tenths of an eV.

We now turn to the evolution of these properties under pressure and chemical substitution. The emerging phase diagram based on our transport measurements of  $T_C$  as a function of the bandgap  $E_G$  in the high-temperature phase shown in Fig. 5 is consistent with the theoretical expectation for the  $T_C$ - $E_G$  dependence<sup>4</sup>, further supporting the excitonic state.  $T_C$  is optimized for the nearly zero-gap semiconductor ( $E_G \sim 0$ )  $\text{Ta}_2\text{NiSe}_5$ . On increasing  $E_G$  in the solid solution  $\text{Ta}_2\text{Ni}(\text{Se}_{1-x}\text{S}_x)_5$ , the excitonic state should be suppressed and switch into a normal semiconductor when  $E_G \sim E_B$ . For  $\text{Ta}_2\text{NiS}_5$  located outside the dome in the phase diagram, the high-temperature (500–550 K) transport activation energy of  $\sim 0.2$  eV, shown in the inset in Fig. 5, implies an energy gap  $E_G$  of  $\sim 0.4$  eV. Recent optical measurements show a similar trend with a gap of  $\sim 0.25$  eV at 350 K measured in  $\text{Ta}_2\text{NiS}_5$  (ref. 23) compared with the effective zero gap in  $\text{Ta}_2\text{NiSe}_5$  (Fig. 3). These results imply that, in contrast to  $\text{Ta}_2\text{NiSe}_5$ ,  $E_G$  in  $\text{Ta}_2\text{NiS}_5$  is larger than  $E_B$ , which has a weaker dependence upon sulfur substitution<sup>23</sup>. These findings are fully consistent with the absence of an excitonic transition in  $\text{Ta}_2\text{NiS}_5$ . In between these limits around  $x = 0.5$ , the energy scale of the bandgap  $E_G$  in the high-temperature phase can

therefore be expected to become comparable with the exciton binding energy  $E_B$  when crossing over from several hundreds of meV in  $\text{Ta}_2\text{NiS}_5$  to effectively zero in  $\text{Ta}_2\text{NiSe}_5$ . This accounts for the stabilization of the excitonic insulator phase around that doping level.

We now turn our attention to the left hand part of the phase diagram. With going to the negative  $E_G$  side with pressure,  $T_C$  goes down with decreasing  $E_G$ . This is consistent with the suppression of the excitonic binding due to the increased screening. The system is approaching the weak coupling BCS regime within the excitonic insulator scenario. Consequently the near-zero-gap  $\text{Ta}_2\text{NiSe}_5$  with the highest  $T_C$  is in the BCS-BEC crossover regime and a relatively strong coupling is anticipated. Indeed, the experimentally obtained  $E_{\text{op}}/k_B T_C \sim 6.5$ , a measure of coupling strength, for  $\text{Ta}_2\text{NiSe}_5$  is much larger than 3.52 for weak coupling BCS, pointing to a moderately strong coupling.

Finally, we are not aware of any other electronically driven mechanism that could give rise to the observed behaviour. Since there is no evidence for magnetic-order scenarios such as Slater- or Mott-insulating phases can be readily excluded. Neither is there any Fermi surface nesting possible that could give rise to a partial gapping of the band structure. Indeed, the excitonic insulator scenario is the only theoretical proposal we are aware of that is consistent with all the observed experimental facts. In particular, the theoretically conjectured dome-shaped phase diagram we observe in this system is the cleanest among all excitonic insulator candidates and therefore represents a key advance in the search for this phase.

In summary, due to the relatively large effective mass of electrons and holes, and the reduced effective dimensionality, the layered direct gap semimetal  $\text{Ta}_2\text{NiSe}_5$  can have a large exciton binding energy of a few tenths of an eV. The separation of electrons and holes confined within the quasi-one-dimensional chains may further help stabilizing the formation of excitons. The optical, transport and specific heat measurements on  $\text{Ta}_2\text{NiSe}_5$  single crystals indicate that the system has an almost zero energy gap at high temperature but, below an electronically driven transition at  $T_C = 326$  K, an excitation gap of  $E_{\text{op}} \sim 0.16$  eV develops. The excitation gap is comparable to the expected exciton binding energy and is reasonably ascribed to the excitonic gap. The electronic phase diagram,  $T_C$  as a function of the energy gap shows a dome-shaped behaviour centred at  $E_G = 0$  expected for an excitonic insulator. Furthermore, the excitonic phase indeed disappears on increasing the energy gap  $E_G$  when  $E_G$  becomes comparable to the exciton binding energy, as expected. Based on this analysis, we conclude that an excitonic state is realized below  $T_C = 326$  K in the nearly zero-gap semiconductor  $\text{Ta}_2\text{NiSe}_5$ .

## Methods

**Sample preparation.** Single crystals of  $\text{Ta}_2\text{NiCh}_5$  (Ch = S, Se and Te) were synthesized by chemical vapour transport. Elemental powders of tantalum, nickel and chalcogens (S, Se and Te) were mixed with a stoichiometric ratio and sealed into an evacuated quartz tube ( $\sim 1 \times 10^{-3}$  Pa) with a small amount of  $\text{I}_2$  as transport agent. The mixture was sintered under a temperature gradient of 950/850 °C. After sintering for 1 week, needle-like single crystals were grown at the cold end of the tube.

**Physical properties measurements.** Electric resistivity and heat capacity measurements were carried out by using a PPMS (Quantum Design). Pressure experiments were carried out using a HPC-33 pressure cell by ElectroLab. High-temperature electronic resistivity was measured by using a bespoke measurement device. Optical parameter were determined using spectroscopic ellipsometry<sup>23</sup>.

**Data availability.** All relevant data are available from the corresponding authors upon request.

## References

- Mott, N. F. The transition to the metallic state. *Phil. Mag.* **6**, 287–309 (1961).
- Halperin, B. I. & Rice, T. M. Possible anomalies at a semimetal-semiconductor transition. *Rev. Mod. Phys.* **40**, 755–766 (1968).
- Kohn, W. Excitonic phases. *Phys. Rev. Lett.* **19**, 439–442 (1967).
- J erome, D., Rice, T. M. & Kohn, W. Excitonic insulator. *Phys. Rev.* **158**, 462–475 (1967).
- Bronold, F. X. & Fehske, H. Possibility of an excitonic insulator at the semiconductor-semimetal transition. *Phys. Rev. B* **74**, 165107 (2006).
- Seki, K. *et al.* Excitonic Bose-Einstein condensation in Ta<sub>2</sub>NiSe<sub>5</sub> above room temperature. *Phys. Rev. B* **90**, 155116 (2014).
- Bucher, B., Steiner, P. & Wachter, P. Excitonic insulator phase in TmSe<sub>0.45</sub>Te<sub>0.55</sub>. *Phys. Rev. Lett.* **67**, 2717–2720 (1991).
- Wachter, P. Exciton condensation in an intermediate valence compound: TmSe<sub>0.45</sub>Te<sub>0.55</sub>. *Solid State Commun.* **118**, 645–650 (2001).
- Wachter, P. The discovery of excitonium. *J. Alloys Compd.* **225**, 133–138 (1995).
- Wilson, J. A. Concerning the semimetallic characters of TiS<sub>2</sub> and TiSe<sub>2</sub>. *Solid State Commun.* **22**, 551–553 (1977).
- Cercellier, H. *et al.* Evidence for an excitonic insulator phase in 1T-TiSe<sub>2</sub>. *Phys. Rev. Lett.* **99**, 146403 (2007).
- Bucher, B., Park, T., Thompson, J. D. & Wachter, P. Thermodynamical signatures of an excitonic insulator. Preprint at <https://arxiv.org/abs/0802.3354> (2008).
- Craven, R. A., Di Salvo, F. J. & Hsu, F. S. L. Mechanisms for the 200 K transition in TiSe<sub>2</sub>: a measurement of the specific heat. *Solid State Commun.* **25**, 39–42 (1978).
- Kaneko, T., Toriyama, T., Konishi, T. & Ohta, Y. Orthorhombic-to-monoclinic phase transition of Ta<sub>2</sub>NiSe<sub>5</sub> induced by the Bose-Einstein condensation of excitons. *Phys. Rev. B* **87**, 035121 (2013).
- Hughes, H. P. Structural distortion in TiSe<sub>2</sub> and related materials—a possible Jahn-Teller effect? *J. Phys. C: Solid State Phys.* **10**, L319–L323 (1977).
- Ishioka, J. *et al.* Chiral charge-density waves. *Phys. Rev. Lett.* **105**, 176401 (2010).
- Sunshine, S. A. & Ibers, J. A. Structure and physical properties of the new layered ternary chalcogenides tantalum nickel sulfide (Ta<sub>2</sub>NiS<sub>5</sub>) and tantalum nickel selenide (Ta<sub>2</sub>NiSe<sub>5</sub>). *Inorg. Chem.* **24**, 3611–3614 (1985).
- Di Salvo, F. J. *et al.* Physical and structural properties of the new layered compounds Ta<sub>2</sub>NiS<sub>5</sub> and Ta<sub>2</sub>NiSe<sub>5</sub>. *J. Less Common Metals* **116**, 51–61 (1986).
- Kaneko, T., Toriyama, T., Konishi, T. & Ohta, Y. Electronic structure of Ta<sub>2</sub>NiSe<sub>5</sub> as a candidate for excitonic insulators. *J. Phys.:Conf. Ser.* **400**, 032035 (2012).
- Greenblatt, M. Molybdenum oxide bronzes with quasi-low-dimensional properties. *Chem. Rev.* **88**, 31–53 (1988).
- Wakisaka, Y. *et al.* Excitonic insulator state in Ta<sub>2</sub>NiSe<sub>5</sub> probed by photoemission spectroscopy. *Phys. Rev. Lett.* **103**, 026402 (2009).
- Zittartz, J. Transport properties of the ‘excitonic insulator’: Electrical Conductivity. *Phys. Rev.* **165**, 605–611 (1968).
- Larkin, T. I. Excitonic Fano resonances in Ta<sub>2</sub>NiSe<sub>5</sub> and Ta<sub>2</sub>NiS<sub>5</sub>. *Online Publikationen der Universit at Stuttgart*. Available at <http://dx.doi.org/10.18419/opus-8843> (2016).
- Matsubayashi, K. Pressure-induced semiconductor-metal transition and superconductivity in Ta<sub>2</sub>NiSe<sub>5</sub>. *CiNii Articles*. Available at <http://ci.nii.ac.jp/naid/110009990261/en> (2015).
- Knox, R. S. Theory of excitons. *Solid State Phys. Suppl* **5**, 100 (1963).
- Klingshirn, C. F. *Semiconductor Optics* (Springer, 2005).

## Acknowledgements

We are grateful for Y. Ohta, T. Kaneko, Y. Katsura and T. Mizokawa for useful discussion. This work was partially supported by Grant-in-Aid for Scientific Research (S; grant no. 24224010) and by Grant-in-Aid for Scientific Research on Innovative Areas (grant no. JP15H05852). H.T. acknowledges support from the Alexander von Humboldt foundation.

## Author contributions

Y.F.L. and T.T. performed synthesis and measurement of physical properties under ambient pressure. H.K., A.W.R. and H.T. collected and analysed the data of transport properties. T.I.L. and A.V.B. measured and analysed the optical conductivity of single crystals. H.T. and B.K. designed and supervised the project. Y.F.L., A.W.R. and H.T. wrote the manuscript with inputs from all authors. All authors discussed and reviewed the paper.

## Additional information

**Supplementary Information** accompanies this paper at <http://www.nature.com/naturecommunications>

**Competing financial interests:** The authors declare no competing financial interests.

**Reprints and permission** information is available online at <http://npg.nature.com/reprintsandpermissions/>

**How to cite this article:** Lu, Y. F. *et al.* Zero-gap semiconductor to excitonic insulator transition in Ta<sub>2</sub>NiSe<sub>5</sub>. *Nat. Commun.* **8**, 14408 doi: 10.1038/ncomms14408 (2017).

**Publisher’s note:** Springer Nature remains neutral with regard to jurisdictional claims in published maps and institutional affiliations.



This work is licensed under a Creative Commons Attribution 4.0 International License. The images or other third party material in this article are included in the article’s Creative Commons license, unless indicated otherwise in the credit line; if the material is not included under the Creative Commons license, users will need to obtain permission from the license holder to reproduce the material. To view a copy of this license, visit <http://creativecommons.org/licenses/by/4.0/>

  The Author(s) 2017